Research Square

Preprints are preliminary reports that have not undergone peer review.
They should not be considered conclusive, used to inform clinical practice,
or referenced by the media as validated information.

The PPAR agonist elafibranor attenuates macrophage reprogramming across diverse silica exposures and limits tissue remodelling

Vivek Dharwal

Vivek.dharwal@addri.org.au

Asbestos and Dust Diseases Research Institute

Richard Zelei

Asbestos and Dust Diseases Research Institute

Ellen Donohoe

Asbestos and Dust Diseases Research Institute

Sakthi Priya Selvamani

Asbestos and Dust Diseases Research Institute

Sharyn Gaskin

Adelaide University

Maaike Kockx

Anzac Research Institute

Caroline Reddel

Anzac Research Institute

Deborah Yates

Asbestos and Dust Diseases Research Institute

Anthony Linton

Asbestos and Dust Diseases Research Institute

Elham Hosseini-Beheshti

Asbestos and Dust Diseases Research Institute

Research Article

Keywords: Silicosis, Macrophages, Peroxisomes, PPAR agonists, Silica Particles, Elafibranor

Posted Date: September 25th, 2026

DOI: https://doi.org/10.21203/rs.3.rs-10814877/v1

License: This work is licensed under a Creative Commons Attribution 4.0 International License.
Read Full License

Additional Declarations: No competing interests reported.

Abstract

Silicosis is a progressive inflammatory lung disease with limited treatment options. Recently, peroxisome signalling has emerged as a key player in inflammation, and the dual PPAR agonist elafibranor has been approved for human use. This study integrates molecular and transcriptomic analyses to compare the effects of silica particles of different sizes (11-nm/500-nm/1-μm) and sources (engineered-stone (ES) and natural-stone (NS)) on macrophages, the primary lung immune responders, and to evaluate elafibranor's therapeutic potential.

Dose and time-course analysis across silica sizes showed that nano-sized silica particles exhibited the highest cellular toxicity. Macrophage phenotype analysis revealed a prominent M1-phenotype (increased *IL-6, CXCL10*, and *TNF-α)*, along with elevated protein carbonyl levels, reduced mitochondrial function, and altered redox homeostasis. Next, transcriptomic profiling showed distinct signatures for each exposure, along with a shared pro-inflammatory response. Consistent with the molecular analysis, nano-sized silica exposure had more pronounced effects than larger particles, and NS induced greater effects than ES. GSEA predicted a significant positive enrichment in multiple pathways, including 'Hallmark_TNFα_Signaling_via_NF-κB ' and 'Hallmark_IL6_JAK_STAT3_Signaling'.

Interestingly, elafibranor treatment reversed silica-induced changes across all tested silica exposures. Our molecular data show that drug treatment was associated with reduced M1 marker expression, diminished ROS production, and attenuated NF-κB signalling. GSEA revealed significant negative enrichment of silica-induced pathways along with positive upregulation of 'Hallmark_Fatty_Acid_Metabolism'.

Furthermore, we evaluated elafibranor's ability to attenuate tissue remodelling driven by silica-reprogrammed macrophages. Our data show that elafibranor treatment significantly downregulated the increased expression of fibrosis markers and inflammatory markers in 2D epithelial and 3D bioprinted epithelial-fibroblast models.

Overall, this study comprehensively characterises immune-molecular signalling in response to diverse silica dusts and provides the first evaluation of a newly approved dual PPAR agonist's efficacy.

1 Introduction

Silicosis is a progressive inflammatory lung disease caused by inhalation of respirable silica dust (Yang, Liu et al. 2025). Studies show that the disease incidence has increased in recent years (Chen, Liu et al. 2022). However, current management strategies mainly focus on alleviating symptoms, leaving the disease's progressive nature largely unaddressed (Leung, Yu et al. 2012, Yang, Liu et al. 2025). Therefore, there is an urgent need to uncover novel mechanisms driving silicosis and identify new therapeutic alternatives.

Briefly, silicosis is classified into four subtypes: chronic simple, chronic complicated, accelerated, and acute, based on clinical symptoms and exposure duration (Lam, Mansell et al. 2022, Yang, Liu et al. 2025). However, little has been explored about the molecular signalling associated with variation in silica particle size and source. The disease pathophysiology involves overlapping stages of parenchymal injury, inflammation, and tissue remodelling. Parenchymal injury occurs when alveolar macrophages (AMs) and epithelial cells phagocytose and endocytose silica particles, respectively. These uptake events can induce cellular injury, release proinflammatory mediators, and lead to redox imbalance. Chronic silica exposure leads to chronic inflammation, which eventually contributes to tissue remodelling and worsening of lung function (Li, Luan et al. 2016, Yu, Fu et al. 2020, Zhao, Li et al. 2024).

Given inflammation's central role in silicosis development and progression, research and therapeutic targeting have primarily focused on established organelles such as mitochondria and lysosomes. The contribution of other organelles remains comparatively unexplored. However, recent studies have highlighted peroxisomes' role in inflammatory signalling (Di Cara, Andreoletti et al. 2019, Di Cara, Savary et al. 2023). Peroxisomes are membrane-bound organelles present in the cytoplasm and contain multiple enzymes associated with biochemical pathways. Growing evidence shows that peroxisome number and protein composition change in response to different stimuli, and that peroxisomes are associated with immunometabolism (Smith and Aitchison 2013, Di Cara, Sheshachalam et al. 2017). Peroxisomal β-oxidation is also linked to the biosynthesis of bioactive polyunsaturated fatty acids, including docosahexaenoic acid and eicosapentaenoic acid. These lipid metabolites have immunosuppressive and anti-inflammatory roles and are key for immune response regulation (Facciotti, Ramanjaneyulu et al. 2012). Studies have shown that peroxisomal docosahexaenoic acid promotes phagosome formation in macrophages, and that 4-phenylbutyric acid-induced peroxisome proliferation alleviates LPS-induced inflammation in them (Di Cara, Sheshachalam et al. 2017, Vijayan, Srinu et al. 2017). Peroxisomes also contain the antioxidant enzyme catalase, which supports redox homeostasis (Fransen, Nordgren et al. 2012).

Given the growing evidence that peroxisomes contribute to inflammation and immune regulation, pharmacological activation of peroxisome proliferator-activated receptors (PPARs) has attracted increasing therapeutic interest for treating inflammatory diseases (Decara, Rivera et al. 2020, Han, Geng et al. 2026). In June 2024, the FDA approved the dual PPAR agonist elafibranor for treating primary biliary cholangitis (a chronic autoimmune disease) in combination with ursodeoxycholic acid (Blair 2024).

Considering all, we designed the present study. Using integrated transcriptomic profiling and molecular analyses, we first compared how silica dust of varied sizes (11nm, 500nm, and 1 μm) and sources (engineered stone (ES) and natural stone (NS)) affect macrophages, the primary immune responders in the lungs. Next, we assessed the efficacy of the newly approved dual PPAR agonist elafibranor in counteracting these effects. Further, we evaluated elafibranor’s ability to attenuate tissue remodelling driven by silica-reprogrammed macrophages using 2D epithelial and 3D bioprinted epithelial-fibroblast

models. This study comprehensively characterises immune-molecular signalling in response to diverse silica dusts and provides the first evaluation of a newly approved dual PPAR agonist's efficacy.

2 Materials and methods

2.1 Cell Culture: The human monocyte cell line THP-1 (Tohoku Hospital Pediatrics) was purchased from ATCC. RPMI 1640 medium (11875-093; Thermo Fisher Scientific) supplemented with 10% FBS and 0.05 mM 2-mercaptoethanol (21985023; Thermo Fisher Scientific) was used to culture these cells. For differentiation, Phorbol 12-myristate 13-acetate (50 ng/mL) was added to RPMI 1640 medium supplemented with 10% FBS, and THP cells in suspension were treated for 72 hours. After incubation, the differentiated cells were washed with PBS and used in subsequent experiments.

Human Bronchial Epithelial Cells (BEAS-2B) were purchased from ATCC. Complete Bronchial Epithelial Cell Growth Medium (CC-3170 BEGM; Lonza) was used to culture these cells. Additionally, the human fibroblast cell line MRC5 was purchased from ATCC. RPMI 1640 medium supplemented with 10% FBS was used to culture them.

2.2 Silica particle and Elafibranor toxicity assays: The toxicity of silica particles to macrophages was determined using the MTT (3-(4,5-Dimethylthiazol-2-yl)-2,5-Diphenyltetrazolium Bromide) assay. Briefly, THP-1 cells were differentiated in 96-well plates as described in Section 2.1. Upon differentiation, the cells were treated with silica particles of different sizes (11nm, 500nm, and 1 µm) and silica dust from AS and NS at 3.125, 6.25, and 25 µg/cm² for up to 72 hours. MTT was added at a final concentration of 5ug/ml, and cells were incubated for 2 hours. The formazan crystals produced were dissolved in 50 µL of DMSO, and absorbance was measured at 540nm.

Additionally, the toxicity of elafibranor (A118286; Merck) was assessed. The drug was dissolved in DMSO, and 20mM stock solutions were stored at -80°C. The working stocks of the drug were prepared in complete RPMI + 10%FBS, and THP-1-derived macrophages were treated at concentrations of 10µM, 15 µM, 30 µM, and 50 µM. MTT assays were performed at 24 hours and 72 hours post-treatment to determine the drug toxicity.

2.3 Treatment of macrophages with silica particles and Elafibranor: Silica particles of different sizes, 11nm (381276; Merck), 500nm (805890; Sigma-Aldrich) and 1 µm (Merck) were purchased. The particles were resuspended in sterile PBS at a stock concentration of 10mg/ml. Additionally, silica dust from natural stone (NS) and Engineered stone (ES) was prepared according to the established method (Ramkissoon, Song et al. 2024). The silica dust generated was resuspended in sterile PBS at a stock concentration of 10mg/ml.

For the treatment of THP-1-derived macrophage cells with silica, the stock silica suspensions were diluted in complete media (RPMI 1640 medium supplemented with 10% FBS). The cells were treated at concentrations of 3.125, 6.25, and 25 µg/cm² for up to 72 hours. For the treatment of THP-1-derived macrophage cells with silica, the stock silica suspensions were diluted in complete media (RPMI 1640

medium supplemented with 10% FBS). The cells were treated at concentrations of 3.125, 6.25, and 25 µg/cm² for up to 72 hours. Additionally, to assess the efficacy of elafibranor, macrophages were treated for 24 hours with normal media, or 11nm silica particles (6.25 µg/cm²) or 11nm silica particles (6.25 µg/cm²) + Elafibranor 30 µM.

2.4 Collection of conditioned media from activated macrophages and treatment of Epithelial cells: THP-1-derived macrophages were cultured in six-well plates. The cells were treated for 24 hours with normal media, or 11nm silica particles (6.25 µg/cm²) or 11nm silica particles (6.25 µg/cm²) + Elafibranor 30 µM. The media supernatant was collected, centrifuged (3000rpm, 10') to remove dead cells and debris, and stored at -80°C.

To analyse the effect of macrophage secretome on epithelial cells, an equal number of BEAS-2B cells were cultured in six-well plates. Once confluent, the cells were treated with the collected CM, which was supplemented with fresh media (CC-3170 BEGM; Lonza) at a 1:1 ratio for 24 hours.

2.5 Development of human 3D Lung tissue model, and treatment with conditioned media:

3D models were printed using a non-contact drop-on-demand commercial 3D bioprinter (RASTRUM, Inventia Life Science). A Dual Matrix Model was used, allowing spatiotemporal separation of fibroblast and epithelial cells, with a portion of overlap enabling direct cell-cell communication. A bioink formulation composed of synthetic peptides GFOGER, RGD, and DYIGSR, and hyaluronic acid was used, yielding a stiffness of 1.1kPa and mimicking the mechanical and biochemical properties of healthy human lung ECM (Inventia Life Science, #Px02.29PH). All bioprinting was performed in a black-walled 96-well plate (Greiner, #655090). Cells were printed at 500,000/mL and 1,500,000/mL for BEAS-2B and MRC5, respectively, corresponding to an initial seeding density of 1,200 BEAS-2B and 3,600 MRC5 per well. 150 µL of BEGM was added to each well immediately following printing. After 24h, the constructs were treated 1:1 with BEGM and secretome from THP-1, THP-1 + SiO2, or THP-1 + SiO2 + 30 µM drug at a final volume of 200 µL per well. Media and treatments were refreshed every 48 h until day 10.

2.5 RNA isolation and cDNA preparation: Total RNA was isolated from THP-1-derived macrophages, BEAS2B cells, and 3D models using a total RNA isolation kit (17200; Norgen Biotek) following the manual instructions. Macrophages were harvested at 6, 24 and 72 hours post-treatment, whereas BEAS2B cells were harvested 24 hours after treatment. The isolated RNA was resuspended in 50 µL RNAase-free water, and purity was analysed spectrophotometrically. The isolated RNA samples were stored at -80°C until further downstream analysis.

The total RNA was processed for cDNA synthesis using the iScript cDNA synthesis kit (1708891; Bio-Rad) according to the manufacturer's instructions. 500ng of initial RNA was used, and the thermal cycler conditions are below: Priming 5' at 25°C, Reverse transcription 20' at 46°C, RT inactivation 1' at 95°C, and hold at 4°C. The cDNA samples were stored at -20°C until further downstream analysis.

2.6 RT-qPCR analysis: Total RNA was isolated from THP cells and BEAS-2B cells treated with different conditions as explained in sections 2.3 and 2.4 using a purification kit (17250, Norgen, Biotech Corp). cDNA was prepared using an iScript cDNA synthesis kit (1708890, Bio-Rad) according to the manufacturer's instructions. Real-time qPCR was performed using SYBR green supermix (KK4600, KAPA SYBR, Merck) and an Applied Biosystems (ViiA 7) detection system. The ΔΔCt method was used for analysis, with β-actin serving as the internal control. The expression levels of *IL-6*, *CXCL10*, *TNF-α*, *IL1β*, *SOD1*, *NOS2*, *MMP2*, *ARG*, *CDK163*, *TGF-β*, *GPX*, and *PRDX* were analysed using predesigned primers (KiCqStart® SYBR® Green Primers, Merck).

2.7 Western blot assays: Western blot analysis was performed on macrophages treated with silica particles and epithelial cells treated with conditioned media from macrophages activated by 11nm silica particles. Briefly, the cells were lysed in 200 µl of ice-cold RIPA with protease and phosphatase inhibitors. Protein concentration was determined using the BCA kit (23225, ThermoFisher Scientific). A total of 30 µg denatured proteins were separated using 10% SDS-PAGE and transferred onto a PVDF membrane. The membranes were blocked with 5% BSA and were incubated with the following primary (monoclonal) and secondary antibodies.

2.7 RNA sequencing and analysis: Total RNA was extracted from THP-derived macrophages following treatment with silica particles (11 nm, 1 µm) and silica dust from NS and ES, with or without drug, for 24 hours. Library preparation utilised the Illumina Stranded Total RNA Prep with Ribo-Zero Plus. Sequencing was performed on the NovaSeq X Plus platform (10B 2×100 bp). Raw FASTQ files were aligned and quantified using the Illumina DRAGEN RNA Analysis platform. For the differential gene expression count matrices, the DESeq2 package in R was utilised. Genes with zero counts were excluded from the analysis, and the genes with an adjusted P value < 0.05 were considered statistically significant. For data visualisation using Heatmaps, the normalised expression values were transformed using the regularised logarithm (rlog) transformation implemented in DESeq2. Heatmaps were generated using the pheatmap package after row-wise standardisation of expression values (scale = "row"), which converts each gene's expression to a Z-score. Genes were hierarchically clustered using Euclidean distance and complete linkage. Heatmaps were exported at 600 dpi for publication. For the gene set enrichment analysis, the clusterProfiler package in R was used. Ensembl gene identifiers were converted to Entrez Gene identifiers using the org.Hs.eg.db annotation database. Genes were ranked by their log2 fold change from the DESeq2 differential expression analysis. The Hallmark gene sets were obtained from the Molecular Signatures Database (MSigDB) using the msigdbr package (Hallmark collection, category H). Enrichment analysis was performed in clusterProfiler using default parameters and a false discovery rate (FDR)- adjusted P-value threshold of 0.05. Normalised enrichment scores (NES) were used to determine the direction and magnitude of pathway enrichment. For KEGG pathway enrichment, the gseKEGG function in clusterProfiler was used. Pathways with an adjusted P value < 0.05 were considered significantly enriched. For the enrichment visualisation using dotplots and enrichment curves, the dotplot() and gseaplot2() functions were used, respectively.

2.8 Cytokine array: To measure the pro-inflammatory effects of silica particles and the efficacy of elafibranor, a cytokine array (ARY005B; R&D Systems) was performed on the secretome from THP-1-derived macrophages, following the manufacturer's instructions. Briefly, THP-1 cells were treated with control media, 11nm silica particles (6.25 µg/cm²), or 11nm silica particles (6.25 µg/cm²) + Elafibranor 30 µM for 24 hours. Post-treatment, the CM was collected, centrifuged, and the protein concentration was determined. For the assay, 500 µL of cell culture supernatant with equal amounts of proteins was used. The chemiluminescent signal from the membranes was detected using Bio-Rad systems, and images were captured at identical exposure times to compare intensities between the samples.

2.9 Protein carbonyl assay (Oxime blot) analysis: Protein carbonyl assay (ab178020) was performed to measure the level of carbonyl groups introduced into proteins, a marker of oxidative stress, upon exposure to silica particles. Briefly, THP-derived macrophages were exposed to silica particles (6.25 µg/cm²; 11nm, 500nm, 1 µm, NS, ES) for 24 hours. Protein lysates were prepared using the extraction buffer, and protein concentrations were measured using the BCA kit (23225, Thermo Fisher Scientific). An equal amount of protein from each treatment group was derivatised with 2,4-dinitrophenylhydrazine (DNPH) according to the user manual to convert carbonyl groups into their corresponding DNP-hydrazone derivatives. The derivatised samples were separated by SDS-PAGE and transferred onto PVDF membranes. Membranes were then probed with an anti-DNP primary antibody followed by the appropriate HRP-conjugated secondary antibody. Immunoreactive bands were visualised using chemiluminescence and quantified by densitometric analysis.

2.10 Mitochondrial membrane potential analysis: Mitochondrial membrane potential was assessed using the JC-1 Assay kit (ab113850; Abcam) following the user manual. THP-1-derived macrophages were seeded in black, flat-bottom 96-well plates. The cells were treated with silica particles of all sizes (as described in Section 2.2) at a concentration of 6.25 µg/cm². Post-treatment, the cells were washed with PBS and incubated with 100 µL/well of 1 µm working JC1 solution for 10 minutes at 37°C. The plates were washed, and fluorescence was detected at 540 nm (excitation) and 590 nm (emission).

2.11 Cellular ROS analysis: Total ROS was analysed in THP-1-derived macrophages using the DCFDA /H2DCFDA - Cellular ROS Assay Kit (ab113851; Abcam) according to the user manual instructions. Briefly, macrophages were seeded in chamber slides and treated with control media, 11nm silica particles (6.25 µg/cm²), or 11nm silica particles (6.25 µg/cm²) + Elafibranor 30 µM for 24 hours. Additionally, some wells were treated with Tert-butyl hydroperoxide (TBHP) at 150 µM for 45 min, which were used as a positive control. Post-treatment cells were washed twice with PBS and incubated with 20 µM DCFDA for 45 minutes at 37°C in the dark. The cells were washed twice with PBS and imaged using a Zeiss Axio Imager M2 with FITC filter settings.

2.12 Statistical analysis: GraphPad Prism (GraphPad Software version 10.3) and R were used for data analysis. For comparison among multiple groups, a one-way ANOVA followed by Sidak's multiple comparison test was performed. $p < 0.05$ was considered significant.

Table 1
List of primary and secondary antibodies:

Company	Name	Animal	Cat. No.
Cell Signaling Technology	Anti-rabbit IgG, HRP-linked Antibody		7074P2
Cell Signaling Technology	Anti-mouse IgG, HRP-linked Antibody		7076
Abcam	Anti-NLRP3 antibody	Rabbit	EPR23094-1
Cell Signaling Technology	BiP (GRP78)	Rabbit	C50B12
Cell Signaling Technology	Cox2 (D5H5)	Rabbit	3177S
Abcam	Anti-Catalase	Rabbit	ab209211
Cell Signaling Technology	Phospho-mTOR (Ser2448)	Rabbit	5536
Cell Signaling Technology	Phospho-NF-kappaB p65 (Ser536)	Rabbit	3033
Cell Signaling Technology	IkappaB alpha (L35A5)	Mouse	4814
Cell Signaling Technology	NF-kappaB p65 (D14E12)	Rabbit	8242
Cell Signaling Technology	Actin	Mouse	8H10D10

3 Results

3.1 Nano-sized silica particles exert greater toxicity, associated with mitochondrial dysfunction, protein damage, and M1 polarisation in macrophages: A time-course study with three doses, 3.125, 6.25, and 25 µg/cm², was performed to assess the toxicity of 11nm, 500nm, and 1 µm silica particles up to 72 hrs. Our data show that 11nm particles at a 25 µg/cm² dose exhibited significant toxicity at the earliest time point (24 hours), which worsened over the time course **(**Fig. 1A**)**. In contrast, at larger sizes, silica doses up to 25 µg/cm² were not significantly toxic even at the 72-hour chronic time point **(Supplementary Fig. 1A-B)**. Based on these observations, 6.25 µg/cm² was selected as a common silica concentration to assess size-dependent effects. Additionally, the toxicity of silica dust collected from ES and NS was evaluated; our data show that no significant toxicity was observed at an equivalent dose (**Supplementary Fig. 1C)**.

Next, we evaluated macrophage polarisation upon exposure to silica. qPCR analysis of M1 and M2 markers shows that 11nm silica particles had a more pronounced pro-inflammatory effect than large particles and equivalent doses of ES and NS. A prominent M1 phenotype was observed, with the greatest inflammatory response at 24 hrs, as reflected by significant increases in *IL-6, CXCL10, TNF-α*, and *IL-1β* **(**Fig. 1B-E **and Supplementary Fig. 2)**. Further, the inflammatory response was associated with redox imbalance, as reflected by a significant increase in protein carbonyl levels, a significant reduction in mitochondrial membrane potential, and significant upregulation of *SOD1* mRNA levels **(**Fig. 1F-H **and**

Supplementary Fig. 3A). Additionally, we assessed the protein levels of catalase, COX2, and p-mTOR; however, no significant trends were observed over the time course (**Supplementary Fig. 3B-C)**.

3.2: Identification of distinct transcriptomic signatures, inflammatory, and metabolic signalling pathways associated with exposure to silica particles of different sizes and sources: To create a comprehensive transcriptomic view of silica-treated macrophages, RNA sequencing was performed. Figure 2A shows the overall set of genes whose expression was significantly altered by silica exposure. In line with our PCR findings, the 11nm-treated groups showed a significantly greater effect than the 1 µm-treated macrophages. Figure 2B **& Supplementary Fig. 4A** show that Inflammatory genes such as *CXCL1, CXCL2, CXCL10, CXCL11, IL32*, and *IL33* were significantly upregulated in the 11nm treated groups. Additionally, redox genes, such as *SOD2* and *HMOX1*, were significantly upregulated. Further parallel increases in expression and activation of proinflammatory transcription factors *STAT1* and *NF-κB1* were observed in most bioactive nano-sized silica particles. As expected, the proinflammatory and redox responses were also associated with increased DNA damage, as reflected by increased *PARP-14* expression.

Next, RNA-seq data for silica dust at equivalent doses from natural and engineered stone were analysed to assess the real-world relevance of our findings. Our data show that NS had a more prominent effect on redox homeostasis in macrophages **(**Fig. 2C**)**. A significant increase in metabolic genes, such as *HSPA6* and *MT-C02*, was observed, indicating a metabolic shift. This was further accompanied by increased oxidative stress (overexpression of *NCF1*, *HMOX1*, and *HGD*) and associated DNA damage (Overexpression of *PARP-3*) (Fig. 2D, **Supplementary Fig. 4B**).

GSEA was performed using the Hallmark and KEGG gene set collections to identify the inflammatory signalling pathways. Figure 3A-D shows the dot plots and enrichment plots for the significantly enriched Hallmark pathways in 11nm vs the control group. In 11nm exposed macrophages, a significant enrichment to the dataset, such as ‘Hallmark_TNA_Signaling_via_NF-κB’, ‘Hallmark_IL6_JAK_STAT3_Signaling’, and ‘Hallmark_Inflammatory_response' was observed. Additionally, non-significant enrichment for Hallmark Oxidative Phosphorylation and fatty acid metabolism was observed, indicating activation of lipid-oxidative and metabolic adaptation programs in the treated macrophages **(**Fig. 3E-G**)**. Further, GSEA to KEGG pathways showed a significant enrichment for IL-17, NF-κB, and TNF signalling pathways **(**Fig. 3H**)**. For the 1µm, ES, and NS groups, similar enrichments were observed; however, in line with the transcriptomic changes, enrichment magnitudes were comparably lower **(Supplementary Figure:4C and 5)**.

3.3: Elafibranor attenuates silica-induced inflammation in macrophages and restores cellular homeostasis: To evaluate the efficacy of elafibranor, multiple doses of the drug were first tested for their toxicity. Our data show that elafibranor, up to 30 µM, was not toxic to macrophages at 24 or 72 hours of treatment **(**Fig. 4A, **Supplementary Fig. 6A)**. Because the most significant effects were observed with 11nm silica particles, subsequent analysis of peroxisomal regulation were conducted using this particle size. Two doses, 15 and 30 µM, were tested to evaluate their ability to reverse silica-induced

inflammatory transcriptional changes in macrophages. Our data show that increased expression of M1 markers *IL-1β, TNF-α, IL-6*, and *CXCL10* was significantly reduced by both drug doses **(**Fig. 4B-E**)**. Next, the effect of elafibranor at the proteome level was assessed. Our data show that, in line with our PCR results, increased protein levels of chemokines MIF, MIP-1, CCL5, and IL-8 were significantly reduced with drug treatment (Fig. 4F). These proteins are associated with monocyte and neutrophil recruitment and are part of the NF–κB–driven inflammatory–fibrotic axis. Additionally, the pro-fibrotic and matrix remodelling regulator Serpin E1 was significantly downregulated (Fig. 4F). Further, we performed live-cell ROS detection using the DCFDA probe. The reduction in inflammatory markers was associated with a decrease in probe signal in the drug-treated group (Fig. 4G).

Since the altered cytokines are associated with NF-κB signalling, the effect of the drug on NF-κB signalling was assessed 60 minutes after silica exposure in the presence or absence of elafibranor. Our results indicate that, while phosphorylation of NF-κB p65 at Ser536 and IκBα levels remained unchanged, total p65 protein abundance decreased, suggesting regulation (Fig. 4I-H). However, given that these measurements were performed at a single early time point, dynamic regulation of canonical NF-κB signalling at other time points cannot be excluded.

3.4: RNA sequencing highlights the molecular signalling associated with the Elafibranor and provides indications of its potential effectiveness across heterogeneous silica exposure conditions: To provide a comprehensive assessment of biological pathways altered by elafibranor, next RNA-sequencing was performed on macrophages treated with silica particles of 11nm, 1 µm, and equivalent doses of dust from natural and engineered stone ± Drug. Figure 5A shows the global transcriptional profile after drug treatment. A conserved transcriptional response to drug treatment was observed, irrespective of silica particle size or source. This reflects the efficacy of peroxisome regulations across multiple exposure conditions. Figure 5B shows the top upregulated and downregulated genes. The top downregulated genes included *CHIC1, C1QA, S100A8, EGFR, SIGLEC1, TLR7, GPR34, VCAM1, GPR82, CD101* associated with inflammation, immune signaling and oxidative stress. Interestingly, *ANGPTL4, LAMB1, SPTA1, SLC40A1, TREML4, CALCRL, HLA-L, TSPAN7, BBOX1-AS1*, and *AKR1B10* were among the upregulated genes with known roles in fatty acid metabolism, tissue repair, and homeostatic regulation. Our GSEA of the Hallmark gene set shows that the pathways upregulated by silica exposure were significantly downregulated by elafibranor treatment. Figure 5C–I shows dot plots and enrichment plots of significantly enriched pathways in macrophages treated with 11 nm silica + Elafibranor vs 11nm silica alone. Drug treatment resulted in significant downregulation of the Hallmark_TNFA_Signaling_via_NF-κB, Hallmark_IL6_JAK_STAT3_Signaling, and Hallmark_Inflammatory_Response pathways, together with upregulation of Hallmark_Fatty_Acid_Metabolism. Similar trends were observed in GSEA analysis on KEGG pathways **(Supplementary Fig. 6B).** GSEA analysis on 1µm, NS, ES treated groups also showed a similar pattern. The reduction of inflammation was associated with significantly enriched oxidative phosphorylation and fatty acid metabolism **(Supplementary Fig. 6C; 7).**

3.5: Elafibranor-driven reprogramming of macrophage secretome suppresses inflammatory and fibrotic remodelling in the epithelial cells and 3D printed lung tissue model: Since tissue scarring and

remodelling are important pathophysiological features of silicosis development and progression, next, the effects of macrophage reprogramming on epithelial cells and 3D printed lung tissues were assessed. As 11nm silica showed the most significant changes in treated macrophages, conditioned media from macrophages treated with 11nm silica ± Elafibranor was used. Acute assessments were performed using 2D-cultured epithelial cells at 24 hours. Our data (Fig. 6B-G) show that CM media from 11nm-treated macrophages significantly increased the gene expression of IL-8, IL-6, and ICAM1 in treated epithelial cells. In contrast, conditioned media from elafibranor-treated macrophages markedly attenuated these pro-inflammatory and adhesion-associated responses. To further validate the macrophage-epithelial inflammatory axis, NLRP3 activation and endoplasmic reticulum stress were examined next. Figure 6H-I shows that elafibranor reduced the expression of GRP78, a heat shock protein, suggesting profound alleviation of endoplasmic reticulum stress and restoration of cellular proteostasis beyond homeostatic conditions.

To evaluate whether these effects translate to a tissue-relevant context, we next assessed the effect using 3D constructs at a chronic time point of 10 days. Figure 6K-O shows that increased expression of fibrosis markers LOXL2 and IL6, and inflammatory markers IL-1b, IL8, ICAM1, and CXCL10, was significantly downregulated by elafibranor treatment. Overall, our data show that macrophage reprogramming ameliorated tissue remodelling associated with silicosis.

4 Discussion

Silicosis is a progressive lung disease caused by exposure to silica dust. Current management strategies mainly focus on alleviating symptoms, and novel therapies are needed. Using integrated molecular and transcriptomic analyses, this study first extensively evaluated the size- and source-dependent effects of silica particles on macrophages, the primary immune responder in the lungs. Next, we tested the efficacy of the recently approved dual PPAR agonist elafibranor against these silica-induced effects. Our data show that distinct transcriptomic signatures were associated with each exposure, and nanosized silica particles had the most prominent effect on macrophages. Interestingly, elafibranor treatment reversed silica-induced transcriptomic changes across all tested particle sizes and sources. Further, elafibranor treatment significantly downregulated silica-reprogrammed macrophage-driven tissue remodelling in 2D epithelial and 3D bioprinted epithelial-fibroblast models. To the best of our knowledge, this study provides the first evaluation of a newly approved dual PPAR agonist's efficacy against silicosis.

Our toxicity analysis shows that the 11nm particles had the highest toxicity even at acute exposure, compared with 500nm and 1 µm particles. These observations align with previous reports (Napierska, Thomassen et al. 2009, Quignard, Mosser et al. 2012, Inoue, Sakamoto et al. 2021). Smaller particles are more likely to cross biological membranes and can induce mitochondrial dysfunction and redox imbalance (Messerschmidt, Hofmann et al. 2016). In addition to heightened toxicity, our pPCR data indicate that 11nm silica particles elicited the most pronounced pro-inflammatory response, as evidenced by a clear M1 macrophage phenotype. The M1 phenotype of macrophages is characterised by increased production of inflammatory cytokines, along with heightened oxidative stress and dysfunction

(Murray and Wynn 2011, Guo, Zhao et al. 2023). We observed a significant increase in markers such as IL-6, CXCL10, and TNF-α, which was associated with reduced mitochondrial membrane potential and elevated protein carbonyl levels. Interestingly, the larger particles (500 nm and 1 μm) elicited a modest inflammatory response and cytotoxicity, but significant alterations in carbonyl levels and mitochondrial membrane potential were observed. This suggests that multiple partially overlapping mechanisms may be involved, depending on particle size. Therefore, safety assessment should not rely solely on toxicity studies or inflammatory endpoints, but should also include mitochondrial dysfunction and oxidative stress.

To gain mechanistic insights into the observed changes, we performed RNA-seq on macrophages exposed to nano-, micro-, NS-, and ES silica. The global transcriptomic analysis highlights a greater magnitude of transcriptional changes induced by 11nm silica particles compared to 1 μm particles. Further, GSEA of Hallmark and KEGG pathways predicts that IL-6, TNF-α, IL-17, JAK-STAT3 and NF-κB signalling pathways are key regulators of the cellular response to silica-induced insults. NF-κB is a family of transcription factors that regulates a wide range of biological functions, including innate and adaptive immune responses, immunometabolism, and more (Li and Verma 2002, Liu, Sun et al. 2024). Studies have shown that NF-κB activation promotes the Warburg effect, a metabolic shift towards glycolysis (O'Neill and Hardie 2013). In our data, we also observed trends toward metabolic alteration; however, they were not statistically significant. Further, transcriptomic analysis of macrophages exposed to NS and ES revealed a more profound response to silica dust from NS. The existing literature reports conflicting findings; however, recent studies highlight the importance of mineral composition, suggesting that silica content should not be the only factor considered when evaluating the toxicity of stone dusts (Grytting, Refsnes et al. 2021, Grytting, Refsnes et al. 2022, Ramkissoon, Song et al. 2024). Therefore, future studies should examine the chemical composition of dust generated from various sources during safety assessments.

After assessing silica-induced cytotoxicity and inflammatory responses, we next investigated whether treatment with the dual PPAR agonist elafibranor can mitigate these changes. Peroxisomes are membrane-bound organelles involved in physiological roles such as fatty acid beta-oxidation, reactive oxygen species regulation, and phospholipid synthesis (Lodhi and Semenkovich 2014, Di Cara, Savary et al. 2023). Recent research shows that, beyond their canonical roles, peroxisomes regulate innate immune pathways by producing immunomodulatory compounds. Peroxisomes produce bioactive lipids such as Docosahexaenoic acid, Eicosapentaenoic acid, Protectins, and lipoxins, which regulate immune cell responses and help resolve inflammation (Di Cara, Andreoletti et al. 2019). Given the growing evidence for peroxisomes in inflammation and immune regulation, pharmacological activation of PPAR receptors has attracted increasing therapeutic interest for treating inflammatory diseases. In June 2024, the FDA approved the dual PPAR agonist elafibranor for treating primary biliary cholangitis (a chronic autoimmune disease) in combination with ursodeoxycholic acid (Blair 2024). Our data showed that elafibranor treatment significantly reduced inflammation and oxidative stress associated with exposure to 11-nm silica particles, which exhibited the greatest cytotoxic and proinflammatory effects among the silica particle sizes examined. We observed anti-inflammatory effects at both the mRNA and protein

levels, as reflected by our qPCR and cytokine assays. Further, our Western blot analysis shows that these effects were associated with NF-κB transrepression. These observations align with previous reports indicating that PPARs act as key regulators of signalling pathways, including NF-κB and JAK/STAT (Van Ginderachter, Movahedi et al. 2008, Chen, Saeed et al. 2023).

To comprehensively evaluate elafibranor efficacy across silica particle sizes and sources, we performed RNA sequencing and transcriptomic analysis of macrophages treated with nano-, micro-, NS-, and ES silica, with or without elafibranor. Our data indicate that elafibranor treatment rescues macrophages against the size- and source-dependent effects of silica particles. GSEA showed that elafibranor treatment significantly reversed silica-induced enrichment of inflammatory pathways, particularly Hallmark_TNFA_signaling_via_NF-κB and Hallmark_IL6_JAK_STAT3_Signaling. These findings support previous studies highlighting the protective effects of PPAR agonists against inflammation and oxidative stress (Liu, Wang et al. 2020, Lee, Yang et al. 2024).

Additionally, our GSEA shows that elafibranor treatment significantly enriched fatty acid metabolism in the treated macrophages. The available literature remains limited, but it highlights that targeting lipid metabolism can be a therapeutic strategy against inflammatory disease (Li, Deng et al. 2026). We now know that intracellular lipid accumulation promotes activation of inflammatory signalling, while lipid catabolism has been associated with an anti-inflammatory response. In macrophages, lysosomal lipogenesis and subsequent fatty acid oxidation are crucial for the development of M2 macrophages (Moore, Sheedy et al. 2013, Ito and Suganami 2024). PPAR agonists have been reported to increase the expression of carnitine palmitoyltransferase 1A (CPT1A) and coactivate peroxisome proliferator-activated receptor gamma coactivator 1-beta (PGC1β), which is linked to increased fatty acid metabolism (Chawla 2010). These studies align with the enrichment of fatty acid metabolism pathways observed in the present study. Therefore, further research should address the role of fatty acid metabolism in silicosis and evaluate its potential as a therapeutic target.

In the context of tissue remodelling associated with silicosis, epithelial and fibroblast cells are the primary cell types involved. Multiple signalling pathways, such as the Notch3–IL18 and TGF-β pathways, are involved (Henderson, Rieder et al. 2020). In this study we evaluated the anti-inflammatory and antifibrotic potential of elafibranor against silica-reprogrammed macrophage-driven tissue remodelling. Given the limitations of 2D cell cultures (as extensively reviewed in our recent literature review), we assessed the drug effects in advanced printed models in addition to the conventional 2D setup (Donohoe, Selvamani et al. 2026). Our data show that elafibranor treatment significantly reduced inflammatory markers and the key remodelling marker LOXL2 in activated epithelial cells and fibroblasts. Lysyl oxidases are a family of proteins that catalyse the conversion of lysine residues into reactive aldehydes involved in ECM crosslinking (Aumiller, Strobel et al. 2017). Studies have shown that inhibiting the YAP-TEAD/LOX signalling axis can reduce pulmonary fibrosis in preclinical models (Wagner, Alsafadi et al. 2025). Additionally, evidence suggests an inverse association between PPAR activation and LOX expression, aligning with our current observations (Subbarayan, Xu et al. 2005). Considering the pivotal

role of LOX signalling in fibrogenesis, future studies will be crucial for advancing the management of fibrotic lung disease.

While this study offers several novel findings, it is important to acknowledge some limitations. Notably, the absence of ex vivo analyses using silicosis patient samples limits the direct clinical relevance of the results. Incorporating such studies in future research would provide a stronger functional validation of the mechanistic insights reported here. In addition, the analysis focused primarily on macrophages; extending the observations to other immune cell types, such as T cells, would provide a more comprehensive view of the drug response.

Overall, our findings strongly suggest that peroxisomal regulation via elafibranor may represent a promising therapeutic strategy for treating silica-induced inflammation and fibrosis.

Declarations

Competing interests:

All authors do not hold any competing interests.

Ethics approval and consent to participate:

Not applicable.

Consent for publication:

Not applicable.

Funding:

This work was supported by the New South Wales State Government with oversight by the Dust Diseases Board.

Author Contribution

V.D.- Conceptualization, Methodology, Investigation, Formal Analysis, Bioinformatics Analysis, Visualization, Writing - Original Draft, and Writing – Review & Editing.R.Z.: Investigation, Formal Analysis, and Writing - Review & Editing.E.D.: Investigation, Formal Analysis, 3D Bioprinting, and Writing – Review & Editing.P.S.: Investigation and Writing - Review & Editing.S.G., M.K., and C.R.: Resources and Writing - Review & Editing.D.Y.: Conceptualization and Writing - Review & Editing.A.L.: Supervision, Project Administration, and Writing - Review & Editing.E.H.B.: Conceptualization, Methodology, Supervision,

Project Administration, and Writing - Review & Editing.All authors reviewed and approved the final manuscript.

Acknowledgements:

The authors gratefully acknowledge Kim Brislane for securing the funding that enabled this work and for her oversight in supporting this research.

Data Availability

The RNA-seq analysis files supporting the data shown in this study are included as a supplementary Excel spreadsheet. The transcriptomic datasets generated during this study will be deposited in a publicly available repository upon acceptance of the manuscript. Accession numbers will be provided before publication.

References

1. Aumiller, V., B. Strobel, M. Romeike, M. Schuler, B. E. Stierstorfer and S. Kreuz (2017). "Comparative analysis of lysyl oxidase (like) family members in pulmonary fibrosis." Sci Rep 7(1): 149.
2. Blair, H. A. (2024). "Elafibranor: First Approval." Drugs 84(9): 1143–1148.
3. Chawla, A. (2010). "Control of macrophage activation and function by PPARs." Circ Res 106(10): 1559–1569.
4. Chen, S., M. Liu and F. Xie (2022). "Global and national burden and trends of mortality and disability-adjusted life years for silicosis, from 1990 to 2019: results from the Global Burden of Disease study 2019." BMC Pulm Med 22(1): 240.
5. Chen, S., A. Saeed, Q. Liu, Q. Jiang, H. Xu, G. G. Xiao, L. Rao and Y. Duo (2023). "Macrophages in immunoregulation and therapeutics." Signal Transduct Target Ther 8(1): 207.
6. Decara, J., P. Rivera, A. J. Lopez-Gambero, A. Serrano, F. J. Pavon, E. Baixeras, F. Rodriguez de Fonseca and J. Suarez (2020). "Peroxisome Proliferator-Activated Receptors: Experimental Targeting for the Treatment of Inflammatory Bowel Diseases." Front Pharmacol 11: 730.
7. Di Cara, F., P. Andreoletti, D. Trompier, A. Vejux, M. H. Bulow, J. Sellin, G. Lizard, M. Cherkaoui-Malki and S. Savary (2019). "Peroxisomes in Immune Response and Inflammation." Int J Mol Sci 20(16).
8. Di Cara, F., S. Savary, W. J. Kovacs, P. Kim and R. A. Rachubinski (2023). "The peroxisome: an up-and-coming organelle in immunometabolism." Trends Cell Biol 33(1): 70–86.
9. Di Cara, F., A. Sheshachalam, N. E. Braverman, R. A. Rachubinski and A. J. Simmonds (2017). "Peroxisome-Mediated Metabolism Is Required for Immune Response to Microbial Infection." Immunity 47(1): 93–106 e107.

10. Donohoe, E., S. P. Selvamani, V. Dharwal, R. Zelei, A. Linton, D. Yates and E. Hosseini-Beheshti (2026). "Tools of the trade: leveraging 3D in vitro models to advance silicosis research." Front Pharmacol 17: 1782408.
11. Facciotti, F., G. S. Ramanjaneyulu, M. Lepore, S. Sansano, M. Cavallari, M. Kistowska, S. Forss-Petter, G. Ni, A. Colone, A. Singhal, J. Berger, C. Xia, L. Mori and G. De Libero (2012). "Peroxisome-derived lipids are self antigens that stimulate invariant natural killer T cells in the thymus." Nat Immunol 13(5): 474–480.
12. Fransen, M., M. Nordgren, B. Wang and O. Apanasets (2012). "Role of peroxisomes in ROS/RNS-metabolism: implications for human disease." Biochim Biophys Acta 1822(9): 1363–1373.
13. Grytting, V. S., M. Refsnes, M. Lag, E. Erichsen, T. S. Rohr, B. Snilsberg, R. A. White and J. Ovrevik (2022). "The importance of mineralogical composition for the cytotoxic and pro-inflammatory effects of mineral dust." Part Fibre Toxicol 19(1): 46.
14. Grytting, V. S., M. Refsnes, J. Ovrevik, M. S. Halle, J. Schonenberger, R. van der Lelij, B. Snilsberg, T. Skuland, R. Blom and M. Lag (2021). "Respirable stone particles differ in their ability to induce cytotoxicity and pro-inflammatory responses in cell models of the human airways." Part Fibre Toxicol 18(1): 18.
15. Guo, C., X. Zhao, R. Ma, L. Zhu, Y. Chen, Z. Yang, Z. Cai, Z. Sun and Y. Li (2023). "Silica nanoparticles promoted pro-inflammatory macrophage and foam cell transformation via ROS/PPARgamma/NF-kappaB signaling." Sci Total Environ 881: 163430.
16. Han, X., Y. Geng, Y. Li, X. Meng and J. Jiao (2026). "Roles of peroxisome proliferator-activated receptors (PPARs) in pancreatic metabolic diseases." Pharmacol Res 227: 108192.
17. Henderson, N. C., F. Rieder and T. A. Wynn (2020). "Fibrosis: from mechanisms to medicines." Nature 587(7835): 555–566.
18. Inoue, M., K. Sakamoto, A. Suzuki, S. Nakai, A. Ando, Y. Shiraki, Y. Nakahara, M. Omura, A. Enomoto, I. Nakase, M. Sawada and N. Hashimoto (2021). "Size and surface modification of silica nanoparticles affect the severity of lung toxicity by modulating endosomal ROS generation in macrophages." Part Fibre Toxicol 18(1): 21.
19. Ito, A. and T. Suganami (2024). "Lipid metabolism in myeloid cell function and chronic inflammatory diseases." Front Immunol 15: 1495853.
20. Lam, M., A. Mansell and M. D. Tate (2022). "Another One Fights the Dust: Targeting the NLRP3 Inflammasome for the Treatment of Silicosis." Am J Respir Cell Mol Biol 66(6): 601–611.
21. Lee, I. T., C. C. Yang and C. M. Yang (2024). "Harnessing peroxisome proliferator-activated receptor gamma agonists to induce Heme Oxygenase-1: a promising approach for pulmonary inflammatory disorders." Cell Commun Signal 22(1): 125.
22. Leung, C. C., I. T. Yu and W. Chen (2012). "Silicosis." Lancet 379(9830): 2008–2018.
23. Li, M., F. Luan, Y. Zhao, H. Hao, Y. Zhou, W. Han and X. Fu (2016). "Epithelial-mesenchymal transition: An emerging target in tissue fibrosis." Exp Biol Med (Maywood) 241(1): 1–13.

24. Li, Q. and I. M. Verma (2002). "NF-kappaB regulation in the immune system." Nat Rev Immunol 2(10): 725–734.
25. Li, Z., W. Deng, L. Yang, C. Tang, J. M. Yue, O. Monteiro, D. T. Baptista-Hon and T. Li (2026). "Lipid metabolism in homeostasis and disease." Signal Transduct Target Ther 11(1): 55.
26. Liu, T. T., H. F. Sun, Y. X. Han, Y. Zhan and J. D. Jiang (2024). "The role of inflammation in silicosis." Front Pharmacol 15: 1362509.
27. Liu, Y., J. Wang, S. Luo, Y. Zhan and Q. Lu (2020). "The roles of PPARgamma and its agonists in autoimmune diseases: A comprehensive review." J Autoimmun 113: 102510.
28. Lodhi, I. J. and C. F. Semenkovich (2014). "Peroxisomes: a nexus for lipid metabolism and cellular signaling." Cell Metab 19(3): 380–392.
29. Messerschmidt, C., D. Hofmann, A. Kroeger, K. Landfester, V. Mailander and I. Lieberwirth (2016). "On the pathway of cellular uptake: new insight into the interaction between the cell membrane and very small nanoparticles." Beilstein J Nanotechnol 7: 1296–1311.
30. Moore, K. J., F. J. Sheedy and E. A. Fisher (2013). "Macrophages in atherosclerosis: a dynamic balance." Nat Rev Immunol 13(10): 709–721.
31. Murray, P. J. and T. A. Wynn (2011). "Protective and pathogenic functions of macrophage subsets." Nat Rev Immunol 11(11): 723–737.
32. Napierska, D., L. C. Thomassen, V. Rabolli, D. Lison, L. Gonzalez, M. Kirsch-Volders, J. A. Martens and P. H. Hoet (2009). "Size-dependent cytotoxicity of monodisperse silica nanoparticles in human endothelial cells." Small 5(7): 846–853.
33. O'Neill, L. A. and D. G. Hardie (2013). "Metabolism of inflammation limited by AMPK and pseudo-starvation." Nature 493(7432): 346–355.
34. Quignard, S., G. Mosser, M. Boissiere and T. Coradin (2012). "Long-term fate of silica nanoparticles interacting with human dermal fibroblasts." Biomaterials 33(17): 4431–4442.
35. Ramkissoon, C., Y. Song, S. Yen, K. Southam, S. Page, D. Pisaniello, S. Gaskin and G. R. Zosky (2024). "Understanding the pathogenesis of engineered stone-associated silicosis: The effect of particle chemistry on the lung cell response." Respirology 29(3): 217–227.
36. Smith, J. J. and J. D. Aitchison (2013). "Peroxisomes take shape." Nat Rev Mol Cell Biol 14(12): 803–817.
37. Subbarayan, V., X. C. Xu, J. Kim, P. Yang, A. Hoque, A. L. Sabichi, N. Llansa, G. Mendoza, C. J. Logothetis, R. A. Newman, S. M. Lippman and D. G. Menter (2005). "Inverse relationship between 15-lipoxygenase-2 and PPAR-gamma gene expression in normal epithelia compared with tumor epithelia." Neoplasia 7(3): 280–293.
38. Van Ginderachter, J. A., K. Movahedi, J. Van den Bossche and P. De Baetselier (2008). "Macrophages, PPARs, and Cancer." PPAR Res 2008: 169414.
39. Vijayan, V., T. Srinu, S. Karnati, V. Garikapati, M. Linke, L. Kamalyan, S. R. Mali, K. Sudan, A. Kollas, T. Schmid, S. Schulz, B. Spengler, T. Weichhart, S. Immenschuh and E. Baumgart-Vogt (2017). "A New

Immunomodulatory Role for Peroxisomes in Macrophages Activated by the TLR4 Ligand Lipopolysaccharide." J Immunol 198(6): 2414–2425.

40. Wagner, D. E., H. N. Alsafadi, N. Mitash, A. Justet, Q. Hu, R. Pineda, C. Staab-Weijnitz, M. Korfei, N. Gvazava, K. Wannemo, U. Onwuka, M. Mozurak, A. Estrada-Bernal, J. Cala-Garcia, K. Mutze, R. Costa, D. Bolukbas, J. Stegmayr, W. Skronska-Wasek, S. Klee, C. Ota, H. A. Baarsma, J. Wang, J. Sembrat, A. Hilgendorff, J. Ding, A. Gunther, R. Chambers, I. Rosas, S. de Langhe, N. Kaminski, M. Lehmann, O. Eickelberg and M. Konigshoff (2025). "Inhibition of epithelial cell YAP-TEAD/LOX signaling attenuates pulmonary fibrosis in preclinical models." Nat Commun 16(1): 7099.
41. Yang, B., X. Liu, C. Peng, X. Meng and Q. Jia (2025). "Silicosis: from pathogenesis to therapeutics." Front Pharmacol 16: 1516200.
42. Yu, Q., G. Fu, H. Lin, Q. Zhao, Y. Liu, Y. Zhou, Y. Shi, L. Zhang, Z. Wang, Z. Zhang, L. Qin and T. Zhou (2020). "Influence of silica particles on mucociliary structure and MUC5B expression in airways of C57BL/6 mice." Exp Lung Res 46(7): 217–225.
43. Zhao, J. H., S. Li, S. L. Du and Z. Q. Zhang (2024). "The role of mitochondrial dysfunction in macrophages on SiO(2) -induced pulmonary fibrosis: A review." J Appl Toxicol 44(1): 86–95.

Figures

Figure 1

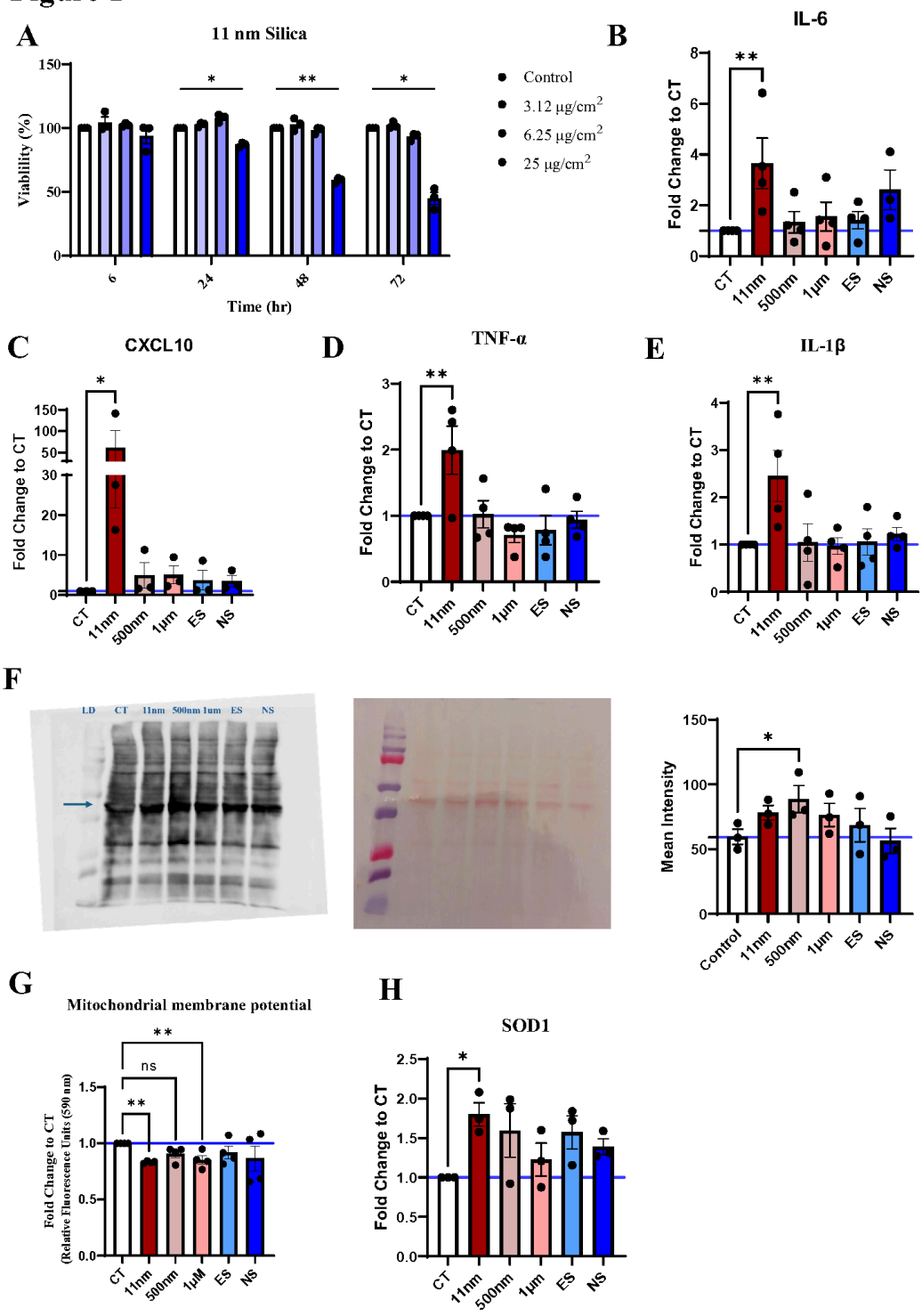


Figure 1

Nano-sized silica particles exert greater toxicity, associated with mitochondrial dysfunction, protein damage, and M1 polarisation in macrophages: THP-1-derived macrophages were treated with three doses (3.125, 6.25, and 25 µg/cm²) of 11nm silica particles up to 72 hrs. Silica particle toxicity, macrophage polarisation, oxidative stress, and mitochondrial dysfunctions were analysed. A) MTT assay assessing cytotoxicity. B–E) qPCR analysis of M1 macrophage phenotype markers IL-6, CXCL10, TNF-α,

and IL-1β. F) Protein carbonyl assessment using OxyBlot. Representative image of Chemiluminescent blot, Ponceau S staining (Loading control), and densitometric analysis. G) Mitochondrial membrane potential quantification using JC-1 dye. H) qPCR analysis of SOD1 as an oxidative stress marker. Data are represented as mean ± SEM; n = 3–4 biological replicates. Statistical analysis was performed using one-way ANOVA followed by Sidak's multiple comparison test. CT: Control/ Untreated macrophages; 11nm: Macrophage treated with 11nm (6.25 μg/cm²) silica particles; 500nm: Macrophage treated with 500nm (6.25 μg/cm²) silica particles; 1 μm: Macrophages treated with 1 μm (6.25 μg/cm²) silica particles; ES: Macrophages treated with engineered stone (ES) dust (6.25 μg/cm²); NS: Macrophages treated with natural stone (NS) dust (6.25 μg/cm²).

Figure 2

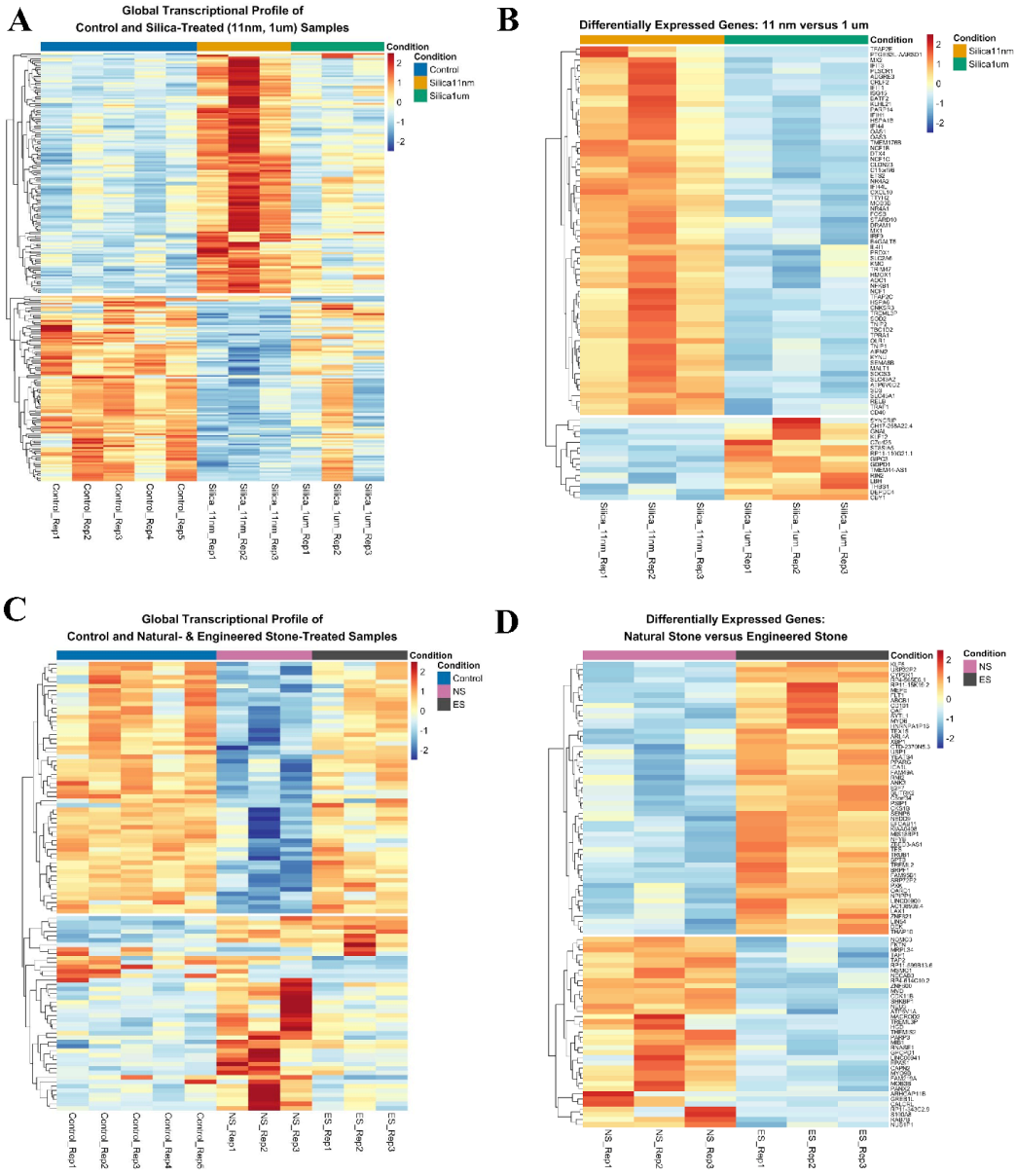


Figure 2

Transcriptional profiling of macrophages exposed to nano- and micro-sized silica particles and dust from natural and engineered stone: THP-1-derived macrophages were treated with 6.25µg/cm² of 11nm and 1 µm, and dust from NS and ES for 24 hours. RNA sequencing was performed, and transcriptional changes were assessed. A) Heat map showing the global transcriptional change in 11nm and 1 µm treated macrophages compared to untreated. B) Heatmap showing the top differentially expressed

genes in 11nm and 1 µm treated macrophages, normalised to control expression. C) Heat map showing the global transcriptional change in NS and ES-treated macrophages compared to untreated. D) Heatmap showing the top differentially expressed genes in NS and ES-treated macrophages, normalised to control expression. n = 3 biological replicates, except for control (n = 5). Control: Untreated macrophages; Silica 11nm: Macrophage treated with 11nm (6.25 µg/cm²) silica particles; Silica 1µm: Macrophages treated with 1 µm (6.25 µg/cm²) silica particles; ES: Macrophages treated with engineered stone dust (6.25 µg/cm²); NS: Macrophages treated with natural stone dust (6.25 µg/cm²).

Figure 3

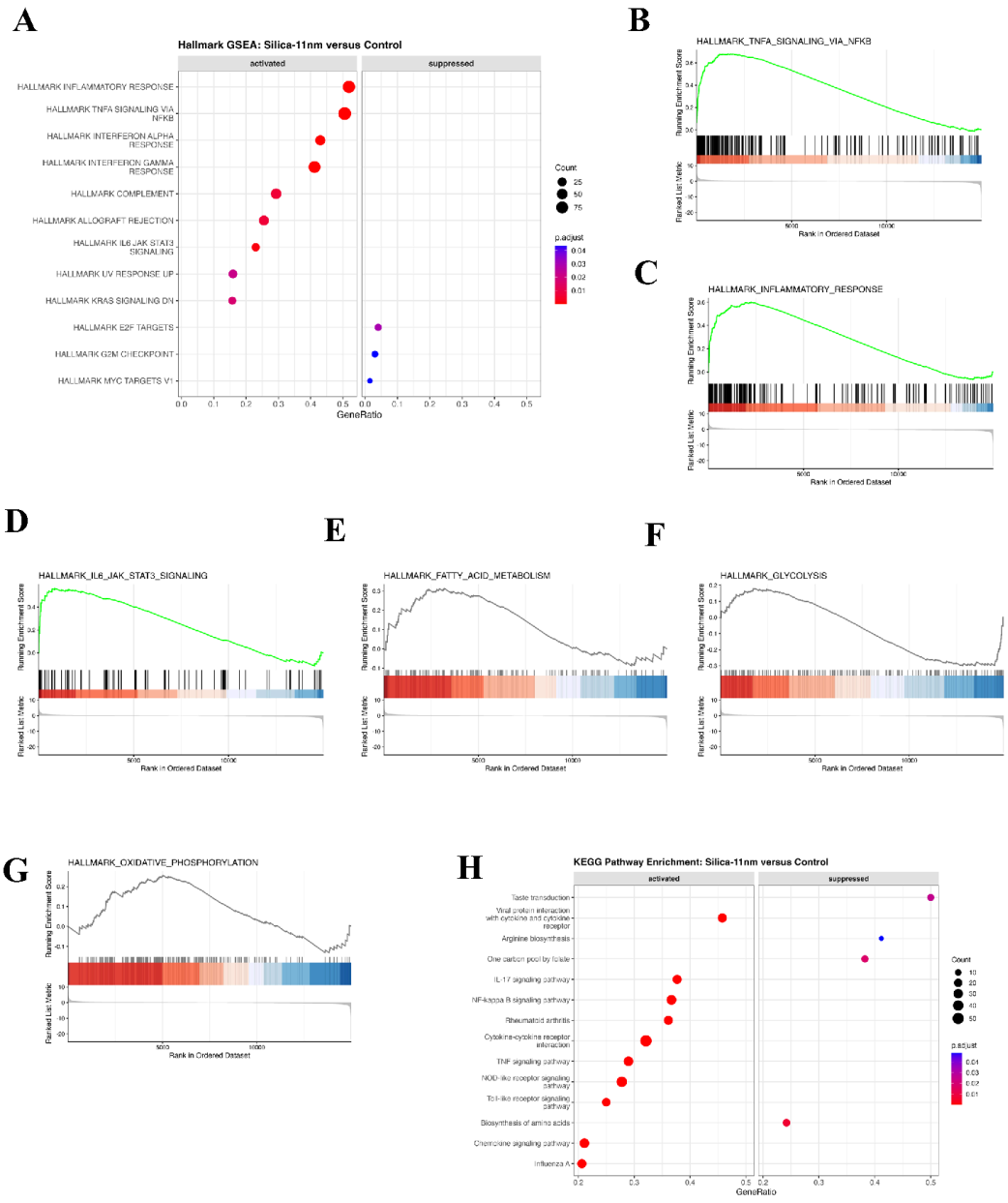


Figure 3

Gene set enrichment analysis (GSEA) for 11nm-silica treated macrophages: THP-1-derived macrophages were treated with 6.25μg/cm² of 11nm for 24 hours. RNA sequencing was performed, followed by differential gene expression and GSEA analysis. A) Dot plot showing significantly enriched Hallmark pathways in macrophages exposed to 11 nm silica, identified by GSEA. B-G) Enrichment plots of selected Hallmark signalling pathways identified by GSEA. H) Dot plot showing significantly enriched KEGG pathways in macrophages exposed to 11 nm silica, identified by GSEA.

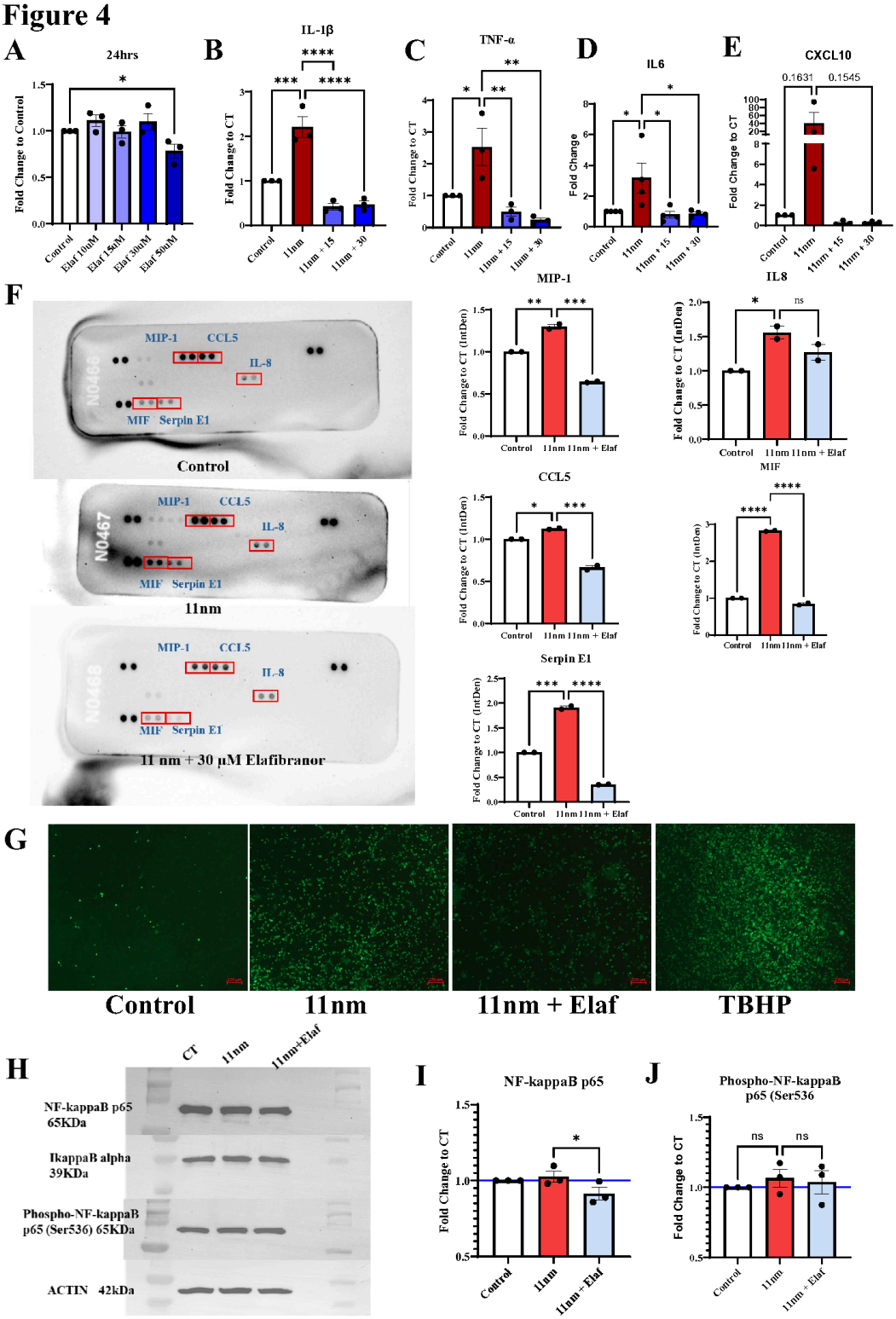


Figure 4

Peroxisomal regulation by Elafibranor ameliorates silica-induced inflammation in macrophages: THP-1-derived macrophages were treated with 6.25µg/cm² of 11nm ± Elafibranor for 24 hours (60 min for NF-κB activation analysis). Assays were performed to evaluate drug toxicity, rescue efficacy, mRNA and proteomic changes, ROS production, and NF-κB activation. A) MTT assay assessing Elafibranor toxicity. B-E) qPCR analysis of M1 macrophage phenotype markers IL-1β, IL-6, TNF-α, and CXCL10. F) Cytokine

array analysis membranes, along with densitometric analysis. G) Representative fluorescence images of intracellular ROS measured using DCFDA staining. TBHP (tert-butyl hydroperoxide) was used as a positive control. Scale-100µm H) Representative chemiluminescent blots for NF-κB activation analysis. (I–J) Densitometric quantification of total NF-κB p65 and phospho-NF-κB p65 (Ser536). Data are represented as mean ± SEM; n = 3 biological replicates. Statistical analysis was performed using one-way ANOVA followed by Sidak's multiple comparison test. Control: Untreated macrophages; 11nm: Macrophage treated with 11nm (6.25 µg/cm²) silica particles; 11nm + 15/30 Elaf: Macrophage treated with 11nm (6.25 µg/cm²) silica particles + Elafibranor (15 or 30 µM).

Figure 5

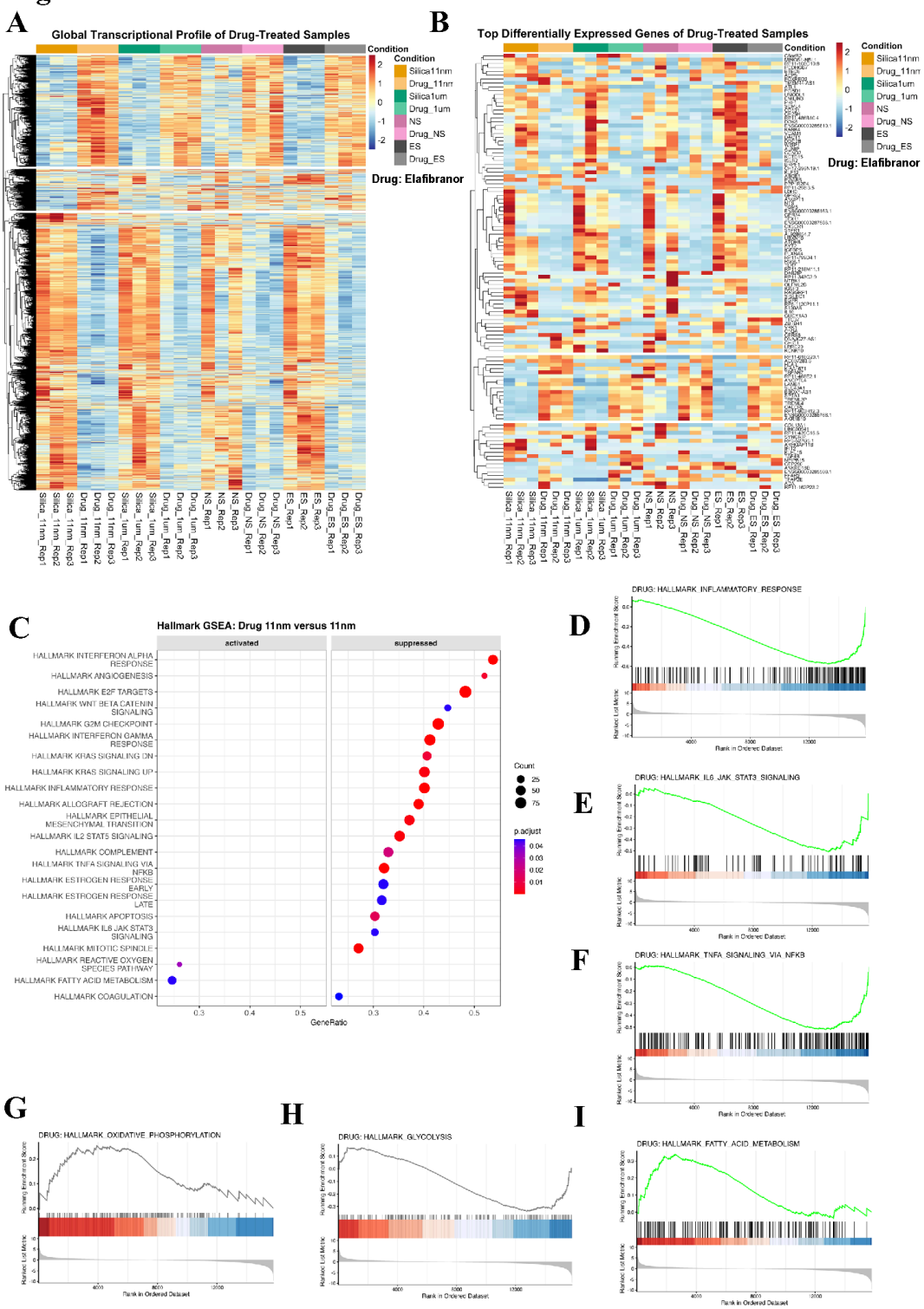


Figure 5

Peroxisomal regulation by Elafibranor, reversed silica-induced transcriptomic alterations across all particle sizes and sources: THP-1-derived macrophages were treated with 6.25µg/cm² of 11nm and 1 µm, and dust from NS and ES ± 30 µM Elafibranor for 24 hours. RNA sequencing was performed, and transcriptional changes were assessed. A) Heat map showing the global transcriptional change in response to different silica exposures and their modulation by Elafibranor. All groups were normalised to

control conditions. B) Heatmap highlighting the top up- and downregulated genes post silica exposures and their modulation by Elafibranor. C) Dot plot showing significantly enriched Hallmark pathways in macrophages exposed to 11 nm silica + 30 µM Elafibranor vs 11 nm silica, identified by GSEA. D-I) Enrichment plots of selected Hallmark signalling pathways identified by GSEA.

Figure 6

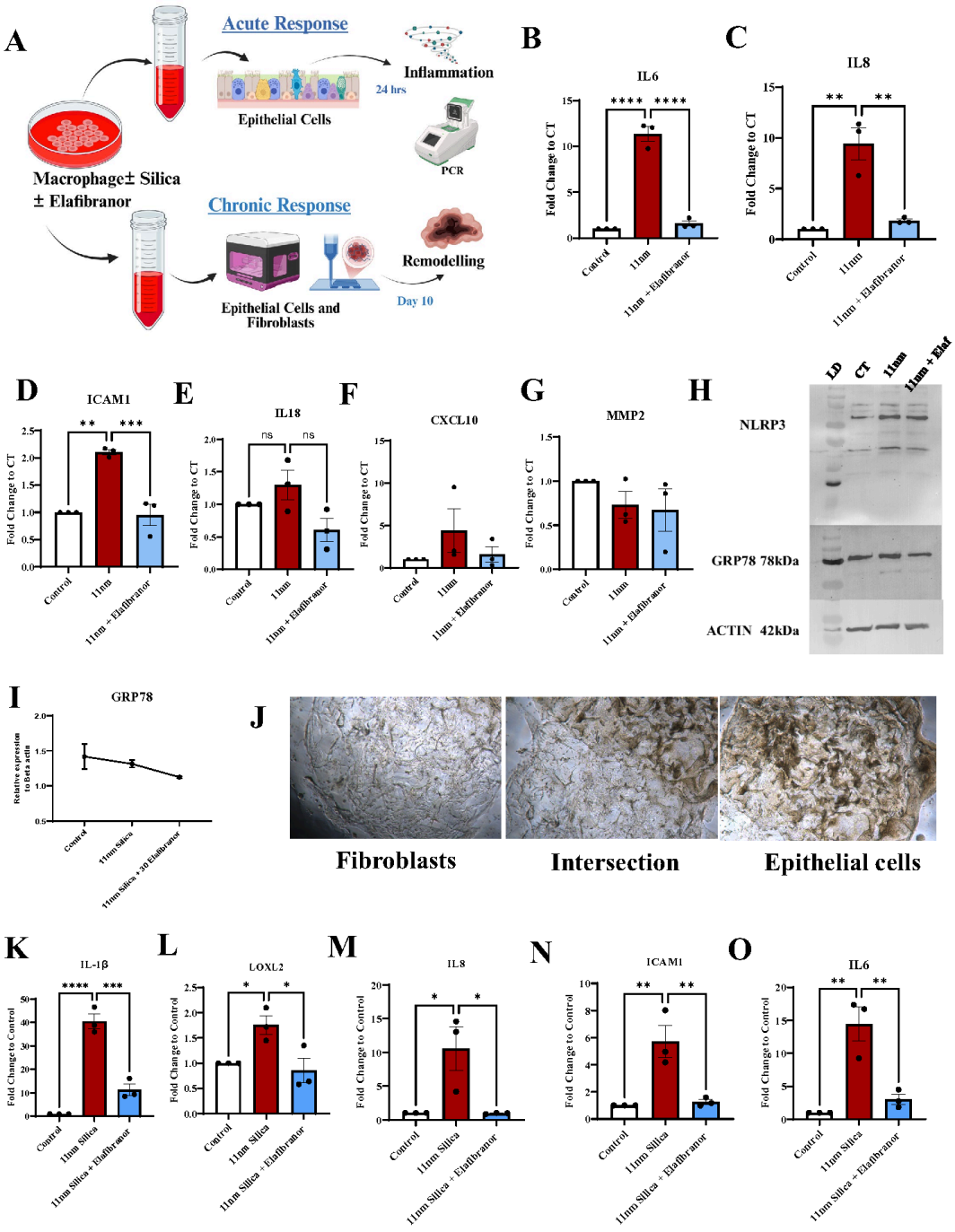


Figure 6

Elafibranor-driven reprogramming of macrophage secretome suppresses inflammatory and fibrotic remodelling in the epithelial cells and 3D printed lung tissue model: A) Schematic presentation showing the treatment of Epithelial cells and 3D printed tissue with macrophage secretome. B-G) qPCR analysis (24hrs) of inflammatory and remodelling markers in epithelial cells cultured in 2D format following indicated exposures. H) Representative chemilinescence blot analysis for NLRP3 activation and GRP78 levels in epithelial cells cultured in 2D format. (n=2) I) Representative image of 3D printer lung tissue model (Day 10). K-0) qPCR analysis of inflammatory and remodelling markers in 3D printer tissue model post different exposures. Data are represented as mean ± SEM; n = 3 biological replicates. Statistical analysis was performed using one-way ANOVA followed by Sidak's multiple comparison test. Control: Untreated macrophages; Silica 11nm: Macrophage treated with 11nm (6.25 µg/cm²) silica particles; Silica 11nm + 30 Elafibranor: Macrophage treated with 11nm (6.25 µg/cm²) silica particles + 30 µM Elafibranor.

Supplementary Files

This is a list of supplementary files associated with this preprint. Click to download.

- SupplementaryFigures.pdf
- SupplementaryTable1.xlsx
- GraphicalAbstract.png